Upper Tropospheric Humidity from MLS and ECMWF Re-analyses

H. L. Clark[1] and R. S. Harwood[1]

16 July 2002

[1]Institute for Meteorology, University of Edinburgh

corresponding author address: Hannah Clark, CNRM, 42 avenue Gaspard Coriolis, 31057 Toulouse Cedex 1, France. hannah.clark@cnrm.meteo.fr

Abstract

This paper compares upper tropospheric humidity from the Microwave Limb Sounder (MLS) on the Upper Atmosphere Research Satellite with European Centre for Medium Range Weather Forecasting (ECMWF) data. MLS measurements are not included in the ECMWF analyses so a comparison of two independent data sets is possible. We focus on the tropical region from 1991–1997 when MLS measurements are available and more specifically from 1991-1994 during the ECMWF 15 year re-analysis period (ERA-15). It is found that the contrast between moist and dry areas, or areas of convection and subsidence is less pronounced in ECMWF data than in MLS. This applies on the scale of both global and regional circulations and results in a semi-annual cycle of high and low correlations between the two data sets which is particularly pronounced over South America. Time-series show the impact of model changes to the absolute values of humidity but make long-term comparison with MLS difficult.

1 Introduction

Water vapor measurements in the upper troposphere are difficult to obtain. In situ measurements from radiosondes, balloons and aircraft are limited in their spatial and global coverage. The radiosonde network has long provided the main source of water vapor observations but radiosondes have limited accuracy in the upper troposphere (e.g., Elliot and Gaffen 1991; Soden and Lanzante 1996). Radiosonde profiles are confined largely to northern hemisphere landmasses with the result that the water vapor field in the upper troposphere, particularly in the tropical region has been poorly observed. Satellites provide a greater spatial and temporal coverage. The Microwave Limb Sounder (MLS) on the Upper Atmosphere Research Satellite (UARS), which is sensitive to water vapor in the upper troposphere (Read *et al.* 1995), provided near global measurements of water vapor from September 1991 to August 1999. It offers several advantages over other satellite instruments. MLS has a vertical resolution of about 3 km in contrast to infrared instruments such as Meteosat (Schmetz and Turpeinen 1988), the US Geostationary Operational Environmental Satellite (GOES) (Soden and Bretherton 1993) and the TIROS Operational Vertical Sounder (TOVS) (Salathé and Chesters 1995), which are sensitive to water vapor in a broad layer of the upper troposphere about 300 hPa thick. The MLS measurement of upper tropospheric humidity is relatively insensitive to cirrus clouds, giving it additional advantages over infrared techniques. The temporal resolution of MLS is better than that of solar occultation instruments such as the Stratospheric Aerosol and Gas Experiment 2 (SAGE II) from which measurements are limited to about 30 per day; MLS makes about 600 measurements per day in the tropical region.

Both satellite and in situ measurements have their advantages and weaknesses and hence they are often combined, or assimilated into a new dataset exploiting the positive aspects of both. Assessing the validity of the assimilated dataset is then difficult since all suitable measurements have gone into its production and hence there are no independent measurements with which it can be compared. The ECMWF re-analysis (ERA-15) humidity fields assimilate data from both TOVS and the radiosonde network and so the MLS data set is useful for comparison with ERA since its observations are not included in the ERA assimilation. In this paper, we compare UARS MLS relative humidity observations at 215 hPa to ECMWF relative humidity data. As already stated, there are likely to be problems in both data sets, ECMWF suffers from a sparse input of data, and MLS has some technical difficulties measuring water vapor in this region (lineshape information cannot be used in the same way for upper tropospheric measurements as for stratospheric measurements (Read *et al.*, 2001). Because of this, we undertake a comparison to cast light on the likely strengths and weaknesses of both datasets. The ECMWF data and MLS data are described in section 2. We discuss time-series of tropical mean values in section 3 and the spatial differences between the two fields in section 4, summarising our conclusions in section 5.

2 Data

a. ECMWF Humidity Analysis

Details of the ECMWF 15-year re-analysis project can be found in Gibson *et al.* (1997). Over most areas of the globe, there are insufficient observations to support

the analysis with the required accuracy. In regions where the data are sparse, the analysis relies upon satellite-based observations. The data assimilation scheme which is used to produce ERA makes use of the ECMWF numerical forecast model to infer information about the state of the atmosphere from data-rich areas to data-sparse areas. Output from the ECMWF forecast model is combined with observations and forcing fields to form the input for the analysis. Results from the analysis, after initialisation, are used as initial conditions for the next forecast and this process is repeated.

The ECMWF analysis assimilates observations from the TOVS satellite and from radiosondes. TOVS consists of three passive vertical sounding instruments, the High-resolution Infrared Radiation Sounder (HIRS-2), the Microwave Sounding Unit and the Stratospheric Sounding Unit (Smith *et al.* 1979). HIRS-2 is a radiometer with 19 channels in the infrared and 1 channel in the visible. HIRS channels 10, 11, and 12 are known as the 'water vapor channels' because variations in humidity strongly affect the measured radiances. The microwave sounding unit has four channels at around 55GHz and the stratospheric sounding unit is an infrared radiometer with three channels near 15μm. Cloud-cleared TOVS radiances were produced by the National Environmental Satellite Data Information Service (NESDIS). The method of 1DVar (Eyre *et al.,* 1993: McNally and Vespirini, 1996) is first used to obtain the atmospheric temperature and humidity profiles which best fit the radiances measured from these channels. The 1DVar temperature retrievals are used globally, over sea areas only, and below 100 hPa. Humidity retrievals from the water vapor channels are used below 300 hPa, over the seas only, and in the tropics, only the cloud free profiles are assimilated.

Radiosonde observations of humidity from below 300 hPa are used in the assimilation but they are not considered accurate enough at the low temperatures and humidities above this height. Hence, above 300 hPa there is no assimilation of water vapor measurements and the analysis is based entirely on 1DVar. In this paper we assess how well the ERA data represents that from MLS at 215 hPa, above the 300 hPa cut-off. We focus primarily on part of the 15 year re-analysis data which overlaps with MLS although some operational data will also be used. The changes to the analysis throughout the operational period will be described where appropriate.

b. MLS data

The UARS satellite, described in Reber (1993), is in an almost circular orbit at an altitude of 585 km and an inclination of 57° to the equator. It makes about 15 orbits a day. MLS makes a limb scan perpendicular to the UARS orbit path from a tangent height of 90 km to the surface and provides a 3 km field of view in the vertical. The measurements of limb radiance from one scan are used to deduce profiles of temperature and of the mixing ratio of various species with the profiles being retrieved onto a fixed pressure grid. MLS has two viewing directions. It looks from 80° N–34° S for about 36 days and then executes a yaw manœvre to look from 34° N to 80° S for another 36 days or so. The tropical region is thus, barring occasional problems with the instrument, observed daily, and measurements are available from 19 September 1991–August 1999. The MLS instrument is described in more detail by Barath *et al.* (1993) and the measurement technique by Waters (1993).

The 205 GHz channel on MLS is principally used to measure chlorine monoxide but it is sensitive to water vapor in the upper troposphere when concentrations are in the range of 100 to 300 ppmv (Read *et al.* 1995). Since the initial retrieval described in *Read et al* (1995), there have been a further two versions released, version 490 (V490) and version 5 (V5) both of which used an improved forward model and a nonlinear least-squares retrieval constrained by the a priori. Full details of the retrievals are described in Read *et al.* (2001). The two more recent versions are drier than the initial version by about 60-70 ppmv (Sandor *et al.* 1998) but are qualitatively similar. The excess humidity in the initial version was caused by an error in the dry-continuum absorption coefficient which was determined from stratospheric radiances and did not extrapolate well into the upper troposphere. Both V490 and V5 used tropospheric radiances to determine the dry and wet absorption coefficient functions.

The main difference between V490 and V5 comes from the determination of the wet component of the absorption coefficient. In V490, the absorption coefficients were calculated from radiances in what is believed to be saturated air and there was an assumed insensitivity to ice emissions. For version 5 however, absorption coefficients were calculated using coincident vaisala radiosonde measurements. More details about the the V490 and V5 measurements can be found in Read *et al.* (2001) and Livesey *et al.*, (2002). Although the retrieval was performed in relative humidity with respect to ice (RHi), the standard V5 level 3at files contain volume mixing ratios which were converted from RHi using NCEP temperatures. We investigate both of these quantities.

Retrievals in the upper troposphere may be affected by thick cirrus clouds. In

the tropical region between 6 and 12 km the retrievals are not significantly affected, but at latitudes poleward 40° a significant fraction of the measured radiances may come from scattering by cirrus clouds (Bond, 1996). Ice crystals in cirrus clouds at a concentration of 0.1 gm^{-3} over a horizontal distance of 120 km could contribute to about 20% of the absorption coefficient at 215 hPa but will usually be less, and at concentrations less than 0.01 gm^{-3} the effect is negligible (Read *et al.* 1995). Ice crystal concentrations of 1 gm^{-3} will emit 20 times more radiation at 203GHz than vapor at 100%RHi. For cirrus associated with a major convective system, such values are not uncommon and have been seen in MLS data. Cirrus which are not associated with convective systems typically have concentrations of 0.003gm^{-3} or less (Knollenberg *et al.,* 1993) and contribute an equivalent of 6% RHi. Since there is expected to be a 20% uncertainty in the continuum functions, thin cirrus are not expected to contribute significantly to MLS UTH errors (Read *et al.* 2001). Values of relative humidity greater than 120% are assumed to be indicative of ice contamination and are reset to 100% in this study as advised in Read *et al.,* (2001).

3 Time-series of Tropical Mean Values

a. Relative Humidity

Figure 1 shows a time-series of MLS relative humidity between 30° N-30° S. To reduce any sampling differences with ECMWF, the data were zonally averaged and the resulting averages area-weighted by the cosine of their latitude. As MLS has aged, it has operated more intermittently. Measurements were made until June 1999 but with an increasing number of missing days. We have less confidence in

the MLS data after 15 June 1997 when the 63GHz radiometer was switched off and changes to the scan pattern were made to conserve spacecraft power (Livesey et al., 2002). The top panel of figure 1 shows the raw data from MLS. The mean of the raw MLS data is 40.3 % with a variance of 7.7%. The variability is made up of natural variability of the atmosphere, random instrument noise and an instrumental artifact associated with the yaw cycle.

The influence of the yaw cycle on the relative humidity measurements is shown in figure 1 (b) which shows an enlarged section of the time-series, chosen to illustrate yaw cycles where the effect is particularly clear. As the ends of a yaw cycle are approached, the antenna receives more radiation from the sun and becomes warmer, affecting the measured radiances. Panel c of figure 1 shows the change in antenna temperature over several yaw cycles. The increase in antenna temperature can be mis-interpreted as a variation in water vapor (at 215 hPa it causes a reduction) as panel (b) reveals. The exact explanation for this is complicated. The antenna temperature varies by about 0.8 K over a yaw cycle and the retrieved relative humidities w.r.t. ice by about 7% (Read *et al.,* 2001). The problem is greater in version 5 than in the previous two versions, worse at 147 hPa (not used in the present study) than at 215 hPa and more evident in mixing ratio than in relative humidity.

We make a linear correction for the yaw cycle based on the 0.8 K variation in antenna temperature and apply this to the raw data. The success of this yaw correction is illustrated in figure 1 (d). The removal of the yaw cycle reduces the variance of this short section of the time-series from 6.3% to 4.7%. The variance of figure 1 (d) is bigger than the precision of the measurements, estimated at 0.6%RHi

for this area average. Some of this difference can be attributed to the day to day variability of the water vapor field and some to remaining variation over the yaw cycle which has not been removed using the simple linear approximation. The yaw correction was applied to the whole time-series and the results are plotted in figure 1(e). This reduces the variance of the time-series from 7.7% to 5.8% but the mean is hardly affected. Corrections for the yaw effect are applied throughout the paper.

We account for any difference resulting from the different vertical resolution of the two datasets by multiplying vertical profiles of ECMWF relative humidities by the MLS averaging kernels in 8 latitude bands (-70,-50,....70). The averaging kernels for MLS are plotted in Read *et al.*, (2001). The effect of multiplying the ECMWF relative humidities by the averaging kernels is small and relatively insignificant compared with other effects as we shall see later.

Figure 2 shows a time-series of all MLS data between 30° N – 30° S with the corresponding ECMWF data, including both the re-analysis and the operational data. ECMWF is the initialised data which has had gravity waves suppressed. As before, the data were zonally averaged first to reduce any sampling discrepancy between MLS and ECMWF, and the resulting averages were area-weighted by the cosine of their latitude.

ERA-15 spans the years January 1979 - February 1994 and provides time-series of consistent meteorological analyses derived from a single version of the ECMWF model. From then on, comparisons with MLS are more difficult. The ECMWF analyses enter a pre-reanalysis mode before switching to the operational analysis on the 4th April 1995. The operational analyses are subject to a wide range of different changes which may or may not have affected the water vapor field and

we illustrate a few here which we imagine to be the most significant. For easy comparison, the time-series are plotted as the variation about the mean, scaled by the mean. Absolute values are indicated on the right-hand axis. Panel (a) shows the MLS relative humidity data after the yaw cycle has been removed as just discussed. Panel b shows the ECMWF relative humidities. The mean of the ECMWF relative humidity time series is 41.4% with a variance of 17.7%. The variance is much larger than MLS, because the ECMWF analyses scheme has been subjected to a number of changes over this period.

The most obvious discontinuity in the ECMWF time-series takes place at the end of the ERA period in 1994 (marked as 'end era' in figure 2c), when the analysis reverted to the mode which was operational in the period before ERA. The ERA system became operational on 4 April 1995 (marked as 'end pre-era'). 3D variational analysis (Courtier *et al.* 1998) was introduced on 30 January 1996 and is marked by the vertical line '3DVar' on figure 2c. Its subsequent modification is also marked. This was followed by the introduction of 4D variational analysis ('4DVar') (Rabier *et al.,* 1998) and by a new version of the Tetens formula to calculate saturation vapor pressure ('new SVP'). The variational analysis code was brought into line with the model, using saturation vapor pressure over water for temperatures above 0° C, over ice for temperatures lower than -23° C and a mixed phase relationship between these two temperatures. Prior to this, the variational analysis code used saturation vapor pressure over ice at temperatures lower than 0° C and over water at temperatures greater than 0° C. The new version of the Tetens formula to calculate SVP was seen to have a significant moistening effect on stratospheric humidity (Simmons *et al.* 1999).

The incorporation of 3- or 4- DVar is important because the analysis of water vapor above 300 hPa contains no direct observations of water vapor and is based entirely on the 1-, 3- or 4- DVar scheme employed. In the stratosphere, the introduction of 3DVar caused a drifting towards unrealistically moist values (Simmons *et al.* 1999). In the upper troposphere 3DVar caused a dramatic drop in relative humidity. The introduction of 4DVar on the other hand, led to a gradual increase of relative humidity. Rabier *et al.* (1998) noted that equatorial averages of humidity for a test period in August 1995 were moister under the 4DVar scheme.

Figure 2e reveals an apparent drop in mixing ratio during boreal summer of 1992, with mixing ratios in the 2nd half of 1992 being lower than those in the 1st half of the year. The drop is also seen in the mixing ratio converted using NCEP temperatures (figure 2 c). We believe the drop to be real and suggest that it may be due to natural interannual variability such as ENSO which is known to affect upper tropospheric water from MLS (Newell *et al.* 1997, Chandra *et al.* 1998) and which led to enhanced moistening during the event of boreal winter 1991/1992 (Waters *et al.* 1999).

Figure 3 shows the rms difference, the bias (MLS-ECMWF) and the correlation calculated for each day of the time-series. The correlation here is between an MLS footprint and the interpolated value from the corresponding ECMWF analysis. It is therefore a measure of the daily spatial correlation between the two fields. This should be independent of any change in bias or linear gain produced by the retrieval or analysis system. We see that the rms difference is generally around 28%RHi. The bias drops by about 7% RHi at the time when the ECMWF analyses revert to their pre-era mode, and both the bias and the rms difference drop after the 16 June

1997 when the 63GHz radiometer was switched off and the scan pattern changed to conserve power. The MLS retrieval became drier but the data remained physically reasonable (Livesey *et al.,* 2002) as is evidenced by the correlation coefficient which does not show any dramatic change. The correlation coefficient ranges from low (0.41) to moderate (0.69) with an average of 0.53. It may be that higher correlations would be achieved if the interpolated ECMWF values were based on more frequent analyses than every 6 hours, but our investigations of the importance of diurnal variations suggest that this effect is small.

It can be noted that the correlation coefficient is not affected by changes to the ECMWF analysis scheme suggesting that the geographical features of the field are preserved and that it is only the bias between the two datasets which changes. The comparative poorness of the correlation indicates that one or other of the two datasets would be unreliable for use in detailed climatological studies, so we look further at the correlation to clarify their relative strengths and weaknesses.

Closer examination of figure 3 reveals that the correlation coefficient exhibits a semi-annual oscillation. Figure 4 shows the correlation over the re-analysis period only, along with the MLS and ERA data, to which the same semi-annual cycle has been fitted. The highest correlations are found in February and August. In the northern hemisphere, the semi-annual oscillation in 300 hPa temperature has its maxima in April/May and October/November and thus coincides with the minimum correlations seen in figure 4. The highest correlations are found when the highest water vapor values have their most extreme displacement from the equator (Wu *et al.,* 1993; Elson *et al.,* 1996). The semi-annual oscillation is strongly evident in the correlation coefficient and MLS values (middle panel) but not in ERA

data (bottom panel). This suggests that some semi-annual pattern is observed by MLS which is not captured by the ECMWF analysis.

A semi-annual oscillation has been previously noted in MLS RHi and MLS mixing ratio fields (Newell *et al.*, 1997; Sandor *et al.*, 1998) and is evident in regions where the inter-tropical convergence zone (ITCZ) crosses the equator twice a year (van Loon and Jenne, 1970). Newell *et al.*, (1997) found that the semi-annual component was largest over land, extending into the Atlantic northeastwards from Brazil. The discrepancy of the two fields may be due to a mismatch in convection over the land-masses or to differences in the position of the ITCZ. Figure 5 shows examples of the two fields at high and low correlation namely, 6th February 1992 and 26th April 1992 respectively. For the 6th February, the similarity between the two fields is obvious but for the 26th April there are some large discrepancies. The MLS field (top) has a region of enhanced moisture over South America which is absent in the ECMWF field. Likewise, MLS shows a region of increased moisture over China and Indonesia which is not revealed by ECMWF. We discuss the difference between the two fields in greater detail in section 4.

b. Mixing Ratio

We now describe some of the differences between the MLS and ECMWF fields which are evident when the relative humidities are converted to mixing ratios. Mixing ratios are converted from RHi using the Clausius Clapeyron equation.

Figure 2 (c) shows MLS mixing ratios calculated using MLS RHi and the NCEP temperatures which give rise to the mixing ratio fields from the standard V5 l3at files. Panel (d) shows ECMWF mixing ratios calculated from ECMWF RHi and

ECMWF temperatures and finally (e) shows mixing ratios from MLS relative humidity and ECMWF temperatures. ECMWF temperatures are linearly interpolated onto 215 hPa to be consistent with the use of NCEP temperatures in the operational production of the MLS l3at files. We can see from this figure that the different temperature fields have a big impact on the deduced mixing ratios.

Firstly, there is a difference in the mean values between panels c and d which show the MLS-NCEP mixing ratios and the ECMWF mixing ratios respectively. MLS-NCEP has a mean of 80 ppmv and ECMWF a mean of 74 ppmv. The mean mixing ratio of MLS-NCEP is reduced when ECMWF temperatures are used to create the mixing ratios from MLS RHi and they become comparable in value to those from ECMWF.

Secondly, we see that the use of different temperature fields has altered the variability of the fields about the mean. The RHi timeseries from MLS shown in panel a has much less variability than either of the two mixing ratios fields calculated from it (c and e). The scaled variance (variance/mean) is 0.14 in panel a compared with 0.34 in c and 0.49 in e. Comparison of panel d and e however shows that not all of the variability comes from the temperature field employed since the temperatures are the same in both of these cases but the variability of d, the ECMWF-ECMWF case is higher (0.91) than that of MLS-ECMWF (0.49)

Thus, the resulting mixing ratios are dependent on the quality of the temperature analyses. These are discussed by Trenberth *et al* (2001.) The NCEP and ECMWF temperature fields are not entirely independent since both include brightness temperatures from MSU. However the MSU temperatures have a stronger influence on the NCEP temperatures than the ERA temperatures because the ERA

temperatures are influenced more strongly by HIRS.

MLS mixing ratios fields calculated using both NCEP and ECMWF temperatures show more variability than the MLS relative humidity. This leads us to consider to what extent the information comes from the MLS retrieval and what extent it is dependent on the the temperature used. The retrieval process requires temperatures in several places. It is found (Read *et al.,* 2001; Read 2002 Personal Communication) that the relative humidity values are insensitive to the adopted temperatures (less so than would be the case for direct retrieval in terms of mixing ratio). The reason is a non-obvious cancellation between the effects of the dependence of saturation mixing ratio on temperature and the effects of the temperature dependence of other parameters in the retrieval, such as the wet and dry continuum absorption coefficients.

We continue to describe the differences between MLS and ECMWF in terms of mixing ratio which has been calculated from relative humidity using the ECMWF temperature fields. Although this means that the two fields are not totally independent, any differences between them must be due to the differences in the relative humidity fields rather than to the temperature fields.

4 Spatial Variations

This section examines the spatial differences between the two water vapor fields. Monthly averages of mixing ratio for MLS and ECMWF are plotted in figures 6 and 7 respectively. Both MLS and ECMWF data have been averaged in 5 °by 5 °bins. Figure 8 shows the difference between MLS and ECMWF monthly means

(i.e. figure 6 minus figure 7). As stated previously, any differences must result from differences in the relative humidity field since the temperatures are the same in both cases.

a. ITCZ and SPCZ

The effects of the Hadley circulation upon upper tropospheric moisture have been widely noted and lead to higher mixing ratios in the tropics than the subtropics. The large-scale ascent within the Hadley circulation is marked by a narrow band of deep cumulus convection which extends across the tropics as the ITCZ. This is well pronounced in figures 6 and 7 as a band of water vapor mixing ratios of 85-115 ppmv lying just north or south of the equator.

In the Eastern Pacific and Atlantic oceans, the ITCZ is located mostly north of the equator at all times of the year. Its most northerly position is about 10° N in June-December in the Pacific, and it lies along the equator in March and April. Over the Indian ocean, the ITCZ is less pronounced as a narrow band. From January to April, the higher mixing ratios are found in the southern hemisphere extending to about 15° S. During northern hemisphere summer, high mixing ratios extend to about 5° S and in the northern hemisphere merge into the Asian monsoon region.

For most of the year the difference plot, figure 8, shows two parallel bands lying north and south of the equator in the central and eastern Pacific, where MLS is observing much drier air than ECMWF. This could result from the ECMWF analyses underestimating the dryness of the descending branch of the Hadley circulation, a feature which has been noted in several previous studies (e.g. Soden and Brether-

ton (1994), Schmetz and van der Berg (1994), Salathé and Chesters, (1995)) and which may contribute to the semi-annual cycle in the correlation coefficient seen in figure 4.

The ITCZ in the Pacific is split into a northern and a southern component known as the South Pacific Convergence Zone (SPCZ). The SPCZ is evident as a band of high mixing ratios extending in a south-easterly direction from New Guinea to about 225° E. The SPCZ appears more distinct from the ITCZ in ECMWF data than in MLS data. This may be due to a greater degree of moistening over the warm pool region which obscures the boundary between the ITCZ and SPCZ in MLS data, and to the reduced horizontal resolution of MLS data compared with ECMWF.

The position and strength of the SPCZ is known to vary seasonally, being most pronounced from December to February and least pronounced between June and August and it also varies on interannual and intraseasonal timescales (e.g. Vincent, 1994). The seasonal variation in position of the SPCZ is exhibited in both MLS and ECMWF datasets. In MLS data, the SPCZ is well marked between October to March, achieving its most eastwards extent to 135° W or 225° E. By comparison, in JJA the SPCZ extends to about 200° E. The seasonal variation in the strength of the SPCZ seems to be less well captured by ECMWF which shows it to be pronounced all year round. Its easterly extent however, shows a similar variation to that of MLS. This tendency for the SPCZ to be a more persistent and well marked feature in the ECMWF model has been noted by Vespirini (1998). Newman *et al.* (2000) however compared ERA data with outgoing longwave radiation (OLR), precipitation and 200 hPa wind divergence from both observations and from two

other re-analysis datasets, the National Center for Environmental Prediction and the National Aeronautics and Space Administration's Goddard Laboratory for Atmospheres. They argued that a double ITCZ was not a feature in the ECMWF fields and that ECMWF compared well with the observations of OLR and precipitation.

High mixing ratios are seen off the coast of Panama during June and July and are replaced from October to March by lower mixing ratios which extend along the coast of South America. This band of dry air lies between the coast of south America and the SPCZ. In both MLS (figure 6) and ECMWF (figure 7) fields, it is a strong feature from September to February when the SPCZ is also strong and the dry band is flanked by moist air. From March to August the dry band and the moist SPCZ are both weaker features. The dry band, as with the SPCZ, is more persistent in the ECMWF data, being evident during northern summer too. This persistence was noted by Vespirini (1998) who attributed it to biased data rather than to a shortcoming of the model. Between August and February, the dry tongue is observed to be moister by ECMWF than by MLS (figure 8). An overestimation of humidity by the ECMWF model in this region was reported by Vespirini (1998) and Soden and Bretherton (1994) when they compared ECMWF with SSM/I. Soden and Bretherton noted that the assimilation of TOVS retrievals in this region may contribute to the problem as a moist bias arises from TOVS total precipitable water content through errors in the cloud clearance method.

b. Continental Centres

There are notable regions of high water vapor mixing ratios which coincide with the well known centres of strong convection over South America and Central Africa. The high mixing ratios are present year round over equatorial Africa. There is some seasonal movement evident over South America with moist air being found around Panama between May and September and over Brazil the rest of the time. These areas of Central and South America and equatorial Africa were observed by Soden and Fu (1995), to have maxima in convection and resulting maxima in upper tropospheric humidity. Figure 8 shows MLS to be wetter over the Brazilian region and drier over Panama during northern winter with the situation reversed in northern summer. This region was noted by Newell *et al.,* (1997) to have a large semi-annual variability.

Figure 9 shows the difference between longitude-time sections of equatorial mixing ratios from MLS and ECMWF (MLS-ECMWF). The longitude-time section was made using a distance weighted interpolation onto grid points spaced every 5°in longitude around the equator (Clark *et al.,* 1998). The position of the land and ocean is clearly reflected in this pattern. MLS is drier than ECMWF (the shaded regions) over the Indian Ocean, Eastern Pacific and Atlantic but wetter than ECMWF in the more convectively active areas of the Western Pacific and the landmasses of Africa and South America. In comparisons with vaisala radiosondes (Read *et al* 2001), MLS V490 was found to be too wet in dry regions and too dry in regions of high RHi. This suggests that the real continent/ocean contrasts may been more extreme than either MLS or ECMWF indicate.

Semi-annual variability can be seen over the Indian ocean, South America and

the Atlantic Ocean. The mismatch in water vapor concentration is particularly evident at 280° E, the edge of South America, from April–June and from September to November when MLS indicates it to be 36 ppmv wetter than ECMWF (hatched regions). At the same times, MLS sees the Indian Ocean to be drier than ECMWF. The difference is smaller during January-March and between August and September which is reflected in the improved correlation coefficients seen in figure 4 at the same times. The mismatch of convection in this region has contributed greatly to the semi-annual oscillation of the correlation coefficient in figure 4.

c. The Asian Monsoon

The Asian monsoon region shows some interesting differences between the two fields. The spatial extent of the moistening associated with the Asian monsoon in JJA is greater in the MLS observations than in the ERA data. The high mixing ratios are located during JJA over India, SE Asia and up to 30° N. A high moisture content remains in the Bay of Bengal until September and moves south eastwards to Indonesia in October. Figure 8 shows the monsoon region to be drier in the ECMWF analyses except during June when we know that MLS was experiencing some problems and there are few valid days in the monthly mean. The subsidence zones which are located to the northwest (over the Arabian peninsula) and south-east (over Australia) of the annual monsoon region are much moister than observed by MLS. The Arabian Peninsula during July, August and September was seen to have low mixing ratio in MLS V490 data at 316, 215 and 147 hPa (Stone *et al.*, 2000). High brightness temperatures, which reveal dry air, were seen by TOVS in this region (Wu *et al.* 1993) particularly in July. Although TOVS data has been

assimilated into the ECMWF model, the Arabian peninsula region is still observed to be drier by MLS and it would seem that the ECMWF analyses fail to capture the moisture contrast between large scale convective and subsidence areas.

5 Conclusions

In this paper we have analysed water vapor from MLS version 5 and from ECMWF. Such a comparison is useful since the MLS measurements are not used in the ECMWF assimilation. The conversion from RHi to mixing ratio highlights the sensitivity to the temperature fields used, with different temperature fields introducing different variability and different absolute values of mixing ratio. Using the same temperature fields for conversion means that the resulting mixing ratio fields are no longer totally independent of each other. Any differences between them however, must then result from the water vapor measurements themselves.

In order to maximise confidence in the MLS measurements and minimise the differences between the two fields due to their different horizontal and vertical resolutions, we prepared the fields for comparison in a number of steps. Although contamination by cirrus is expected to be small, we reset MLS RHi values greater than 120% back to 100%. We accounted for the difference in vertical resolution between the two datasets by multiplying vertical profiles of ECMWF RHi by the MLS averaging kernels. The yaw cycle effect in MLS data was removed using a simple linear approximation to the antenna radiance change. Finally, the measurements were zonally averaged and given an area weighting to try and account for the sampling difference between ECMWF and MLS.

Despite making these adjustments there remain significant differences between the two fields. On a daily basis, spatial correlations between MLS and ECMWF are low (0.53) and exhibit a semi-annual cycle, with the correlation coefficient improving during February and August when the ITCZ has its most extreme displacement from the equator. A longitude-time section showed there to be a semi-annual disparity in moisture concentration over South America with the maximum difference occurring from April-June and from September-November. The correlations during these periods was particularly low.

We have found that there is a lack of contrast between dry and moist areas, or areas of convection and subsidence. MLS indicates greater moisture content in the air over convectively active regions and much drier air than ECMWF over oceanic areas and area where motion is expected to be downwards such as northwest and southeast of the Asian monsoon. This is in agreement with other studies and thus it would appear that the strength of both global and regional circulations is not sufficiently well captured by ECMWF.

This paper illustrates the necessity for accurate global measurements of water vapor and we await the completion of ERA-40 analysis and the launch of the Earth Observing System Microwave Limb Sounder (EOS MLS) to enable a more comprehensive study of the variability of water vapor over longer time-scales.

Acknowledgements

We thank Bill Read for many useful comments. This work was funded by NERC.

6 References

Barath, F., et al. 1993: The Upper Atmosphere Research Satellite Microwave Limb Sounder Instrument. *J. Geophys. Res*, **98,** 10751–10762

Bond, S., 1996: The Potential effect of cirrus on microwave limb sounder retrievals, Ph.D Thesis, University of Edinburgh.

Chandra, S.,J. R. Ziemke, W. Min, and W. G. Read, 1998: Effects of 1997–1998 El Niño on tropospheric ozone and water vapor *Geophys. Res. Letts.* **25** 3867–3870

Clark, H. L.,R. S. Harwood, P. W. Mote, and W. G. Read, 1998: Variability of water vapor in the tropical upper troposphere as measured by the Microwave Limb Sounder on UARS. *J. Geophys. Res.*, **103,** 31695–31707

Courtier, P.,E. Andersson, W. Heckley, J. Pailleux, D. Vasiljević, M. Hamrud, A. Hollingsworth, F. Rabier, and M. Fisher, 1998: The ECMWF implementation of three-dimensional variational assimilation (3D-Var).I:Formulation. *Q. J. R. Meteorol. Soc.* **124** 1783–1807.

Elliot, W. P., D. J. Gaffen, 1991: On the utility of radiosonde humidity archives for climate studies *Bull. Am. Meteorol. Soc.*, **72,** 1507–1520

Elson, L. S., W. G. Read, J. W. Waters, P. W. Mote, J. S. Kinnersley, and R. S. Harwood, 1996: Space-time variations in water vapor as observed by the UARS Microwave Limb Sounder *J. Geophys. Res.* , **101**, 9001–9015.

Eyre, J. R., G. Kelly, A. P. McNally, E. Andersson,and A. Persson, 1993: Assimilation of TOVS radiances through one-dimensional variational analysis. *Q. J. R. Meteorol. Soc.*, **119,** 1427–1463

Gibson, J. K., P. Kallberg, S. Uppala, A. Hernandez, A. Nomura, E. Serrano, 1997: ERA description', ECMWF re-analysis Project Report Series 1.

Knollenberg, R.G., K. Kelly, J.C. Wilson, 1993: Measurements of high number densities of ice crystals in the tops of cumulonimbus, *J. Geophys. Res.* **98**, 8639–8664.

Livesey, N. J., W. G. Read, L. Froidevaux, J. W. Waters, H. C. Pumphrey, D. L. Wu, M. L. Santee, Z. Shippony, R. F. Jarnot, 2002: The UARS Microwave Limb Sounder version 5 dataset: Theory, characterization and validation," J. Geophys. Res., *submitted to J. Geophys. Res.* .

McNally, A. P. and M. Vespirini, 1996: Variational analysis of humidity information from TOVS, *Q. J. R. Meteorol. Soc* **122,** 1521–1544

Newell, R.E., Y. Zhu, W.G. Read, J.W. Waters, 1997: Relationship between tropical upper tropospheric moisture and eastern tropical Pacific sea surface temperature at seasonal and interannual time scales, *Geophys. Res letts.*, **24**, pp 25–28.

Newman, M., P. D. Sardeshmukh, and J. W. Bergman, 2000: An assessment of the NCEP, NASA and ECMWF reanalyses over the tropical west Pacific warm pool, *Bull. Amer. Meteorol. Soc.*, **81**, 41–48

Rabier, F., J-N. Thépaut, P. Courtier, 1998: Extended assimilation and forecast experiments with a four-dimensional variational assimilation system *Q. J. R. Meteorol. Soc.* **124** 1861–1887.

Read, W. G., J. W. Waters, D. A. Flower, L. Froidevaux, R. F. Jarnot, D. L. Hartmann, R. S. Harwood, R. B. Rood, 1995: Upper tropospheric water vapor from UARS MLS. *Bull. Am. Meteorol. Soc.*, **76,** 2381–2389

Read, W. G., J. w. Waters, D. L. Wu, E. M. Stone, Z. Shippony, A. C. Smedley, C. C. Smallcomb, S. Oltmans, D. Kley, H. G. J. Smit, J. L. Mergenthaler, and M. K. Karki, 2001: UARS MLS Upper Tropospheric Humidity Measurement: Method and Validation *J. Geophys. Res.*, **in press.** page–page

Reber, C. A. 1993: The Upper Atmosphere Research Satellite (UARS). *Geophys. Res. letts.,* **20,** 1215–1218

Salathé, E. P., D. Chesters, 1995: Variability of moisture in the upper troposphere as inferred from TOVS satellite observations and the ECMWF model analysis in 1989. *J. Climate*, **8,** 120–132

Sandor, B. J., W. G. Read, J. W. Waters, and K. H. Rosenlof, 1998: Seasonal Behaviour of Tropical to Mid-Latitude Upper Tropospheric Water Vapor from UARS MLS. *J. Geophys. Res*, **103**, 25935–25947

Schmetz, J. and L. van de Berg, 1994: Upper tropospheric humidity observations from Meteosat compared with short-term forecast fields. *Geophys. Res. Letts.*, **21,** 573–576

Schmetz, J., O. M. Turpeinen, 1988: Estimation of the upper tropospheric humidity field from METEOSAT water vapor image data *J. Appl. Meteorol.*, **27,** 889–899

Simmons A. J., A. Untch, C. Jakob, P. Kallberg, and P. Unden, 1999: Stratospheric water vapor and the tropical tropopause temperatures in ECMWF analyses and multi-year simulations *Q. J. R. Meteorol. Soc* **125** 353–386

Smith, W. L., H. M. Woolf, C. M. Hayden, D. Q. Wark, L. M. and McMillin, 1979: The TIROS -N Operational Vertical Sounder, *Bull. Am. Meteorol. Soc.*, **60,**

1177–1187

Soden, B. J., F. P. Bretherton, 1994: Evaluation of water vapor distribution in General Circulation Models using satellite observations. *J. Geophys. Res*, **99,** 1187–1210

Soden, B. J., F. P. Bretherton, 1993: Upper-tropospheric relative humidity from the GOES 6.7 μm channel: Method and climatology for July 1987 *Journal of Geophys. Res.* , **98,** 16669–16688

Soden, B. J., J. R. Lanzante, 1996: An assessment of satellite and radiosonde climatologies of upper-tropospheric water vapor *J. Climate*, **9,** 1235–1250

Soden, B. J., R. Fu, 1995: A satellite analysis of deep convection, upper tropospheric humidity and the greenhouse effect. *J. Climate*, **8,** 2333–2351

Stone, E. M., L. Pan, B. J. Sandor, w. G. Read, and J. w. Waters, 2000: Spatial distributions of upper tropospheric water vapor measurements from the UARS Microwave Limb Sounder *J. Geophys. Res*, **105,** 12149–12161

Trenberth, K. E., D. P. Stepaniak, J. W. Hurrell, 2001: The quality of reanalyses in the tropics, *J. Climate*, **14**, 1499–1510.

van Loon, H., R.L. Jenne, 1970: On the half-yearly Oscillations in the Tropics, *Tellus*, **22**, pp 391–398.

Vespirini, M. 1998: Humidity in the ECMWF model: Monitoring of operational analyses and forecasts using SSM/I observations. *Q. J. R. Meteorol. Soc* **124,** 1313–1327

Vincent, D. G. 1994: The South Pacific Convergence Zone (SPCZ): A Review. *Monthly Weather Review*, **122,** 1949–1970

Waters, J. W. 1993: *Microwave Limb Sounding, Atmospheric Remote Sensing by Microwave Radiometry*, Wiley

Waters, J. W., W. G. Read, L. Froidevaux, R. F. Jarnot, R. E. Cofield, D. A. Flower, G. K. Lau, H. M. Pickett, M. L. Santee, D. L. Wu, M. A. Boyles, J. R. Burke, R. R. Lay, M. S. Loo, N. J. Livesey, T. A. Lungu, G. L. Manney, L. L. Nakamura, V. S. Perun, B. P. Ridenoure, Z. Shippony, P. H. Siegel, R. P. Thurstans, R. S. Harwood, H. C. Pumphrey, M. J. Filipiak, 1999: The UARS and EOS Microwave Limb Sounder Experiments, *J.Atmos. Sci.* **56** , 194–218

Wu, X., J. J. Bates, and S. J. Khalsa, 1993: A climatology of the water vapor brightness temperatures from NOAA operational satellites. *J. Climate*, **6,** 1282–1300

Figure 1: (a) Time-series of raw MLS version 5, 30° N–30° S averaged relative humidity measurements. Vertical lines indicate the region which has been expanded to form (b). (c) The change in calibrated radiance over a yaw cycle. (d) Yaw corrected version of (b). In a and c the crosses represent north looking days and the squares, south looking days. (e) is the the yaw correction applied to the whole time-series in (a).

Figure 2: Time-series 30°N and 30°S averaged water vapor (a), MLS RHi with the yaw cycle removed (see fig 1) (b), the equivalent days from ECMWF RHi showing changes to the ECMWF analysis scheme, (c), MLS mixing ratios formed using the NCEP temperatures (d) ECMWF mixing ratios formed from ECMWF temperatures and (e) MLS mixing ratios formed from ECMWF temperatures. Left-hand axes are plotted as variation from the mean and scaled by the mean. Right-hand axes give approximate absolute values.

Figure 3: Time-series of daily rms difference (top), bias (middle) and correlation (bottom) for MLS and ECMWF relative humidity in the 30° N-30° S region.

Figure 4: Top panel shows the spatial correlation between MLS and ECMWF RHi in the region 30° N-30° S, over the reanalysis period. A semi-annual cycle has been fitted. Middle and bottom panels show 30° N-30° S averaged MLS and ECMWF RHi data with the same semi-annual fit.

Figure 5: Days with above average (6th February 1992) and below average (26 April 1992) correlation between MLS (top) and ECMWF (bottom) fields. Correlations are 0.68 and 0.46 respectively.

Figure 6: Monthly averaged MLS mixing ratio (ppmv) at 215 hPa for January–December 1992. Mixing ratios have been produced from relative humidity using the ECMWF temperatures.

Figure 7: Monthly averaged ECMWF mixing ratio (ppmv) at 215 hPa for January–December 1992. ECMWF relative humidities were multiplied by the MLS vertical averaging kernel and ECMWF temperatures were used in conversion to mixing ratio as in figure 6.

Figure 8: MLS minus ECMWF monthly averaged mixing ratio (ppmv) at 215 hPa for January–December 1992.

Figure 9: Longitude-time section showing the difference (MLS-ECMWF) in mixing ratio at the equator and 215 hPa. Contour interval is every 12 ppmv with values less than zero shaded, and values greater than 36 ppmv hatched.

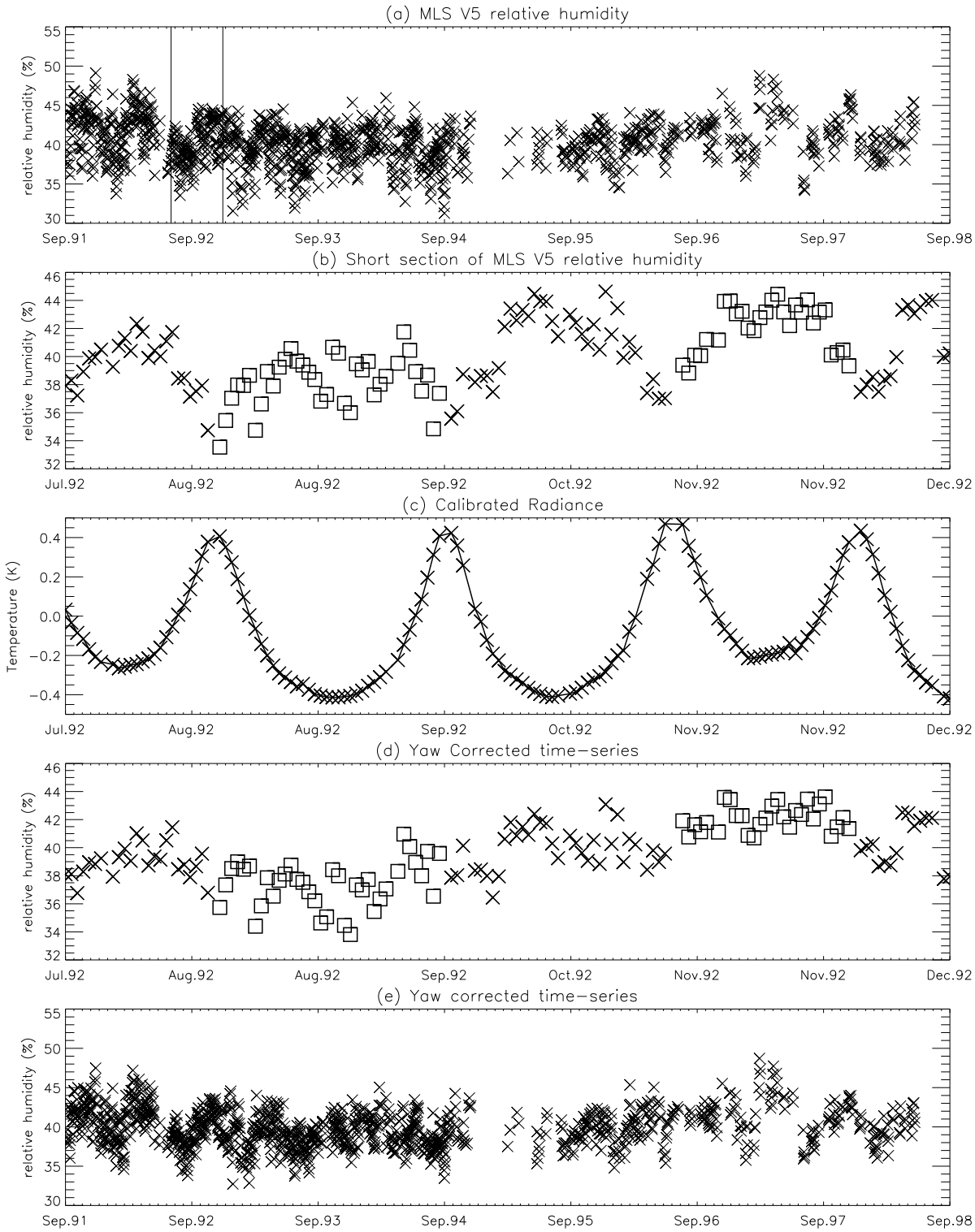
(a) MLS V5 relative humidity
relative humidity (%)
55
50
45
40
35
30
Sep.91
Sep.92
Sep.93
Sep.94
Sep.95
Sep.96
Sep.97
Sep.98
(b) Short section of MLS V5 relative humidity
relative humidity (%)
46
44
42
40
38
36
34
32
Jul.92
Aug.92
Aug.92
Sep.92
Oct.92
Nov.92
Nov.92
Dec.92
(c) Calibrated Radiance
Temperature (K)
0.4
0.2
0.0
−0.2
−0.4
Jul.92
Aug.92
Aug.92
Sep.92
Oct.92
Nov.92
Nov.92
Dec.92
(d) Yaw Corrected time−series
relative humidity (%)
46
44
42
40
38
36
34
32
Jul.92
Aug.92
Aug.92
Sep.92
Oct.92
Nov.92
Nov.92
Dec.92
(e) Yaw corrected time−series
relative humidity (%)
55
50
45
40
35
30
Sep.91
Sep.92
Sep.93
Sep.94
Sep.95
Sep.96
Sep.97
Sep.98

Figure 1: Time-series of raw MLS version 5, 30° N–30° S averaged relative humidity measurements. Vertical lines indicate the region which has been expanded to form (b). (c) The change in calibrated radiance over a yaw cycle. (d) Yaw corrected version of (b). In a and c the crosses represent north looking days and the squares, south looking days. (e) is the the yaw correction applied to the whole time-series in (a).

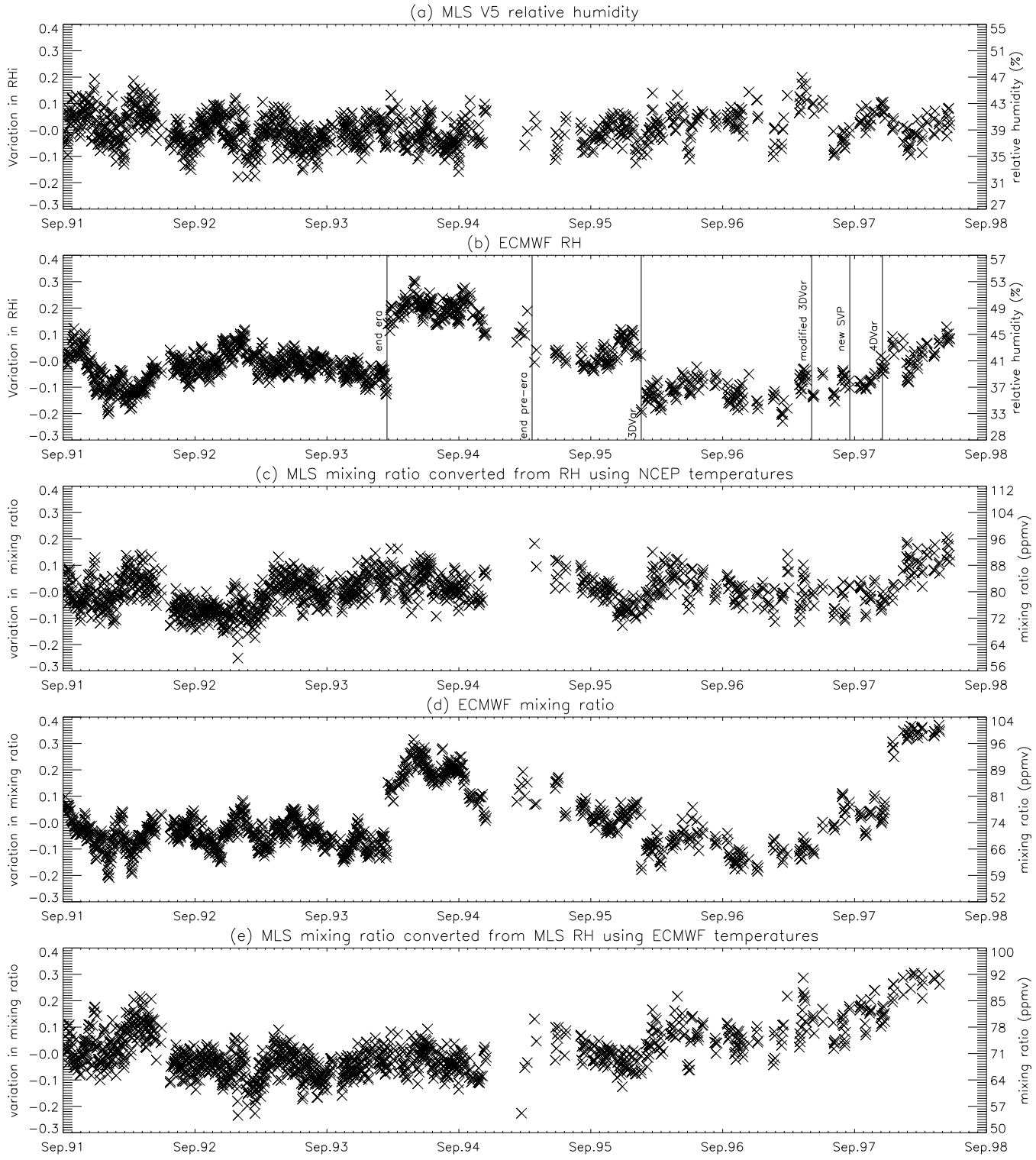
(a) MLS V5 relative humidity
Variation in RHi
relative humidity (%)
(b) ECMWF RH
end era
end pre−era
3DVar
modified 3DVar
new SVP
4DVar
(c) MLS mixing ratio converted from RH using NCEP temperatures
variation in mixing ratio
mixing ratio (ppmv)
(d) ECMWF mixing ratio
(e) MLS mixing ratio converted from MLS RH using ECMWF temperatures
Sep.91
Sep.92
Sep.93
Sep.94
Sep.95
Sep.96
Sep.97
Sep.98

Figure 2: Time-series of 30°N and 30°S averaged water vapor (a), MLS RHi with the yaw cycle removed (see fig 1) (b), the equivalent days from ECMWF RHi showing changes to the ECMWF analysis scheme, (c), MLS mixing ratios formed using the NCEP temperatures (d) ECMWF mixing ratios formed from ECMWF temperatures and (e) MLS mixing ratios formed from ECMWF temperatures. Left-hand axes are plotted as variation from the mean and scaled by the mean. Right-hand axes give approximate absolute values.

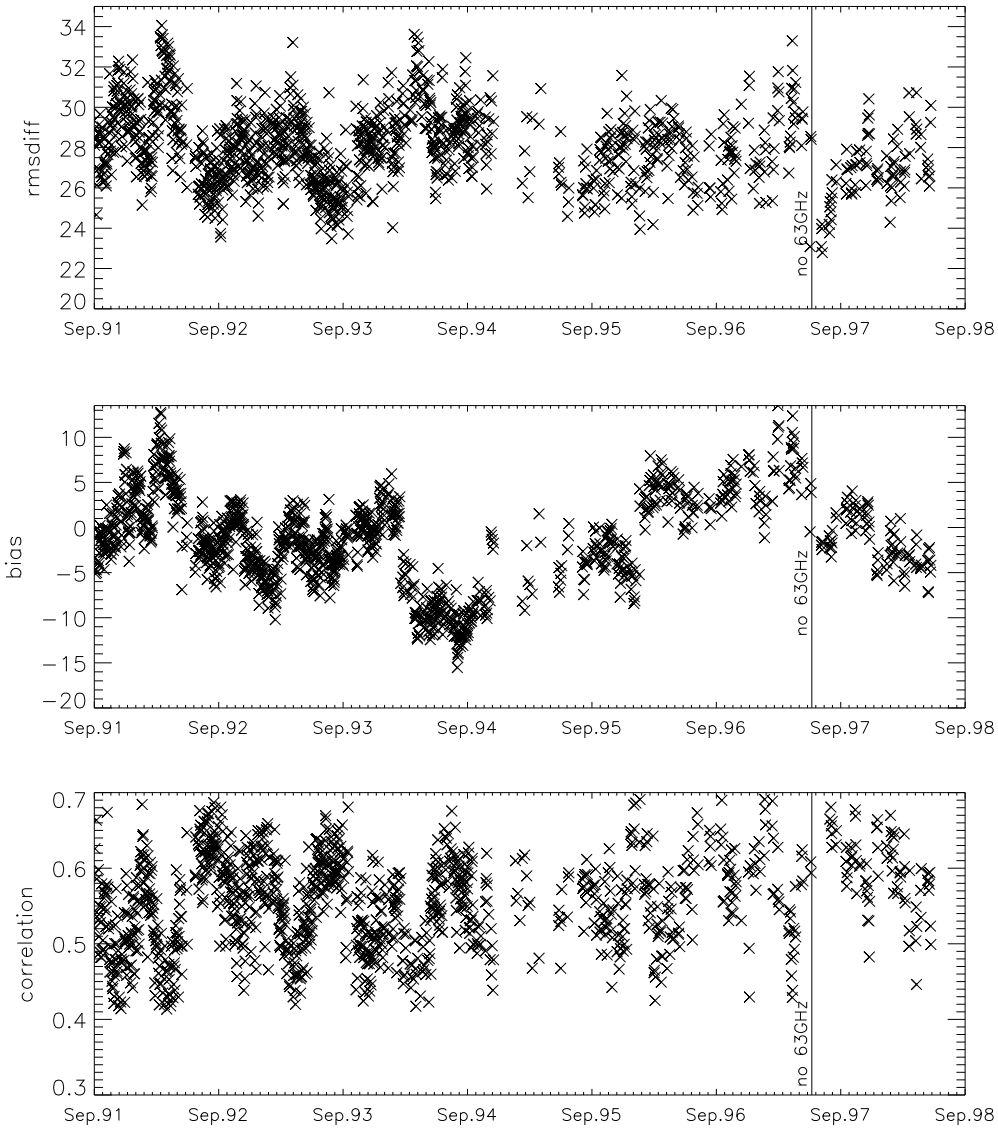
rmsdiff
34
32
30
28
26
24
22
20
no 63GHz
Sep.91
Sep.92
Sep.93
Sep.94
Sep.95
Sep.96
Sep.97
Sep.98
bias
10
5
0
−5
−10
−15
−20
no 63GHz
Sep.91
Sep.92
Sep.93
Sep.94
Sep.95
Sep.96
Sep.97
Sep.98
correlation
0.7
0.6
0.5
0.4
0.3
no 63GHz
Sep.91
Sep.92
Sep.93
Sep.94
Sep.95
Sep.96
Sep.97
Sep.98

Figure 3: Time-series of daily rms difference (top), bias (middle) and correlation (bottom) for MLS and ECMWF relative humidity in the 30° N-30° S region.

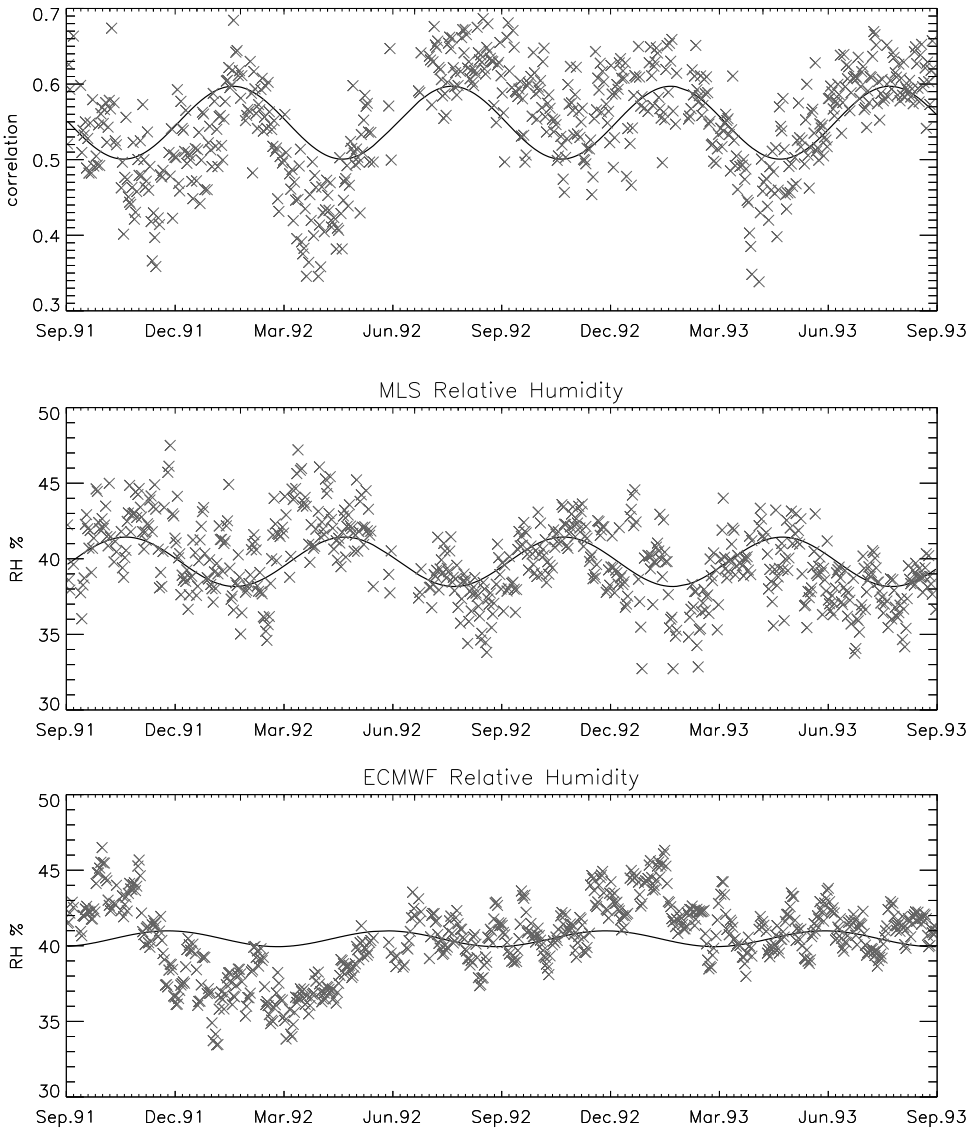
correlation
0.7
0.6
0.5
0.4
0.3
Sep.91
Dec.91
Mar.92
Jun.92
Sep.92
Dec.92
Mar.93
Jun.93
Sep.93
MLS Relative Humidity
RH %
50
45
40
35
30
ECMWF Relative Humidity

Figure 4: Top panel shows the spatial correlation between MLS and ECMWF RHi in the region 30° N-30° S, over the reanalysis period. A semi-annual cycle has been fitted. Middle and bottom panels show 30° N-30° S averaged MLS and ECMWF RHi data with the same semi-annual fit.

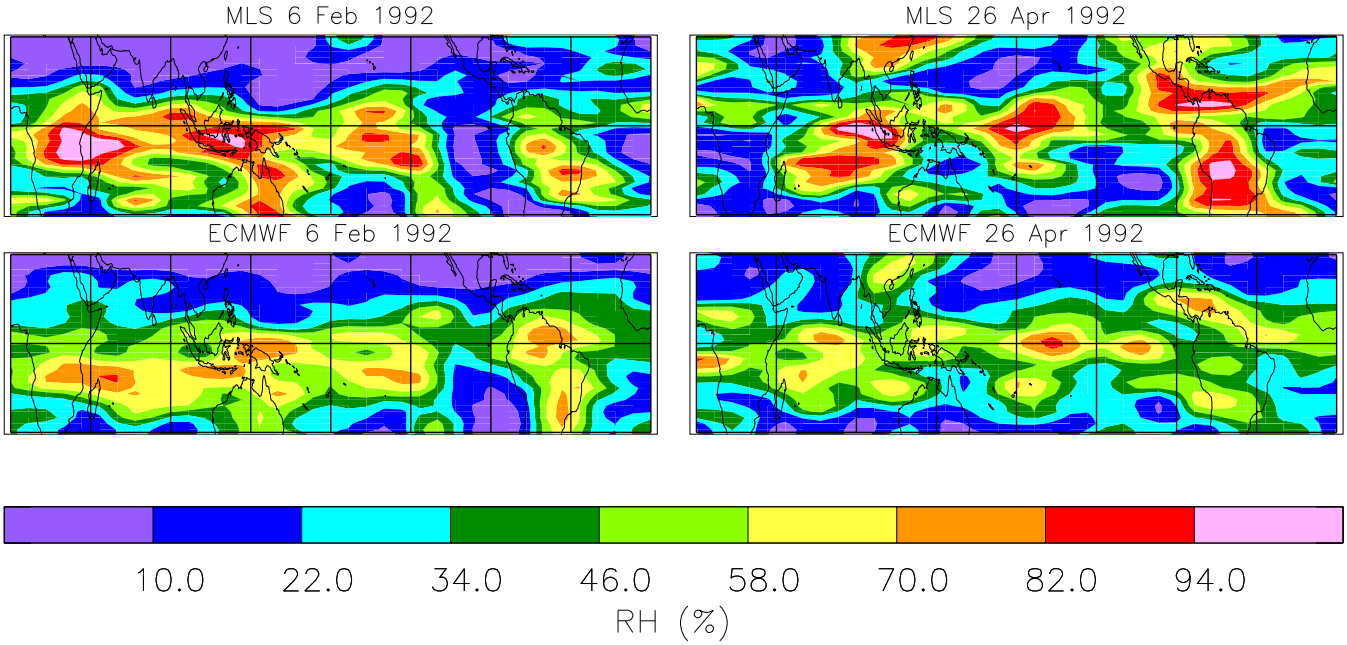
MLS 6 Feb 1992
MLS 26 Apr 1992
ECMWF 6 Feb 1992
ECMWF 26 Apr 1992
10.0
22.0
34.0
46.0
58.0
70.0
82.0
94.0
RH (%)

Figure 5: Days with above average (6th February 1992) and below average (26 April 1992) correlation between MLS (top) and ECMWF (bottom) fields. Correlations are 0.68 and 0.46 respectively.

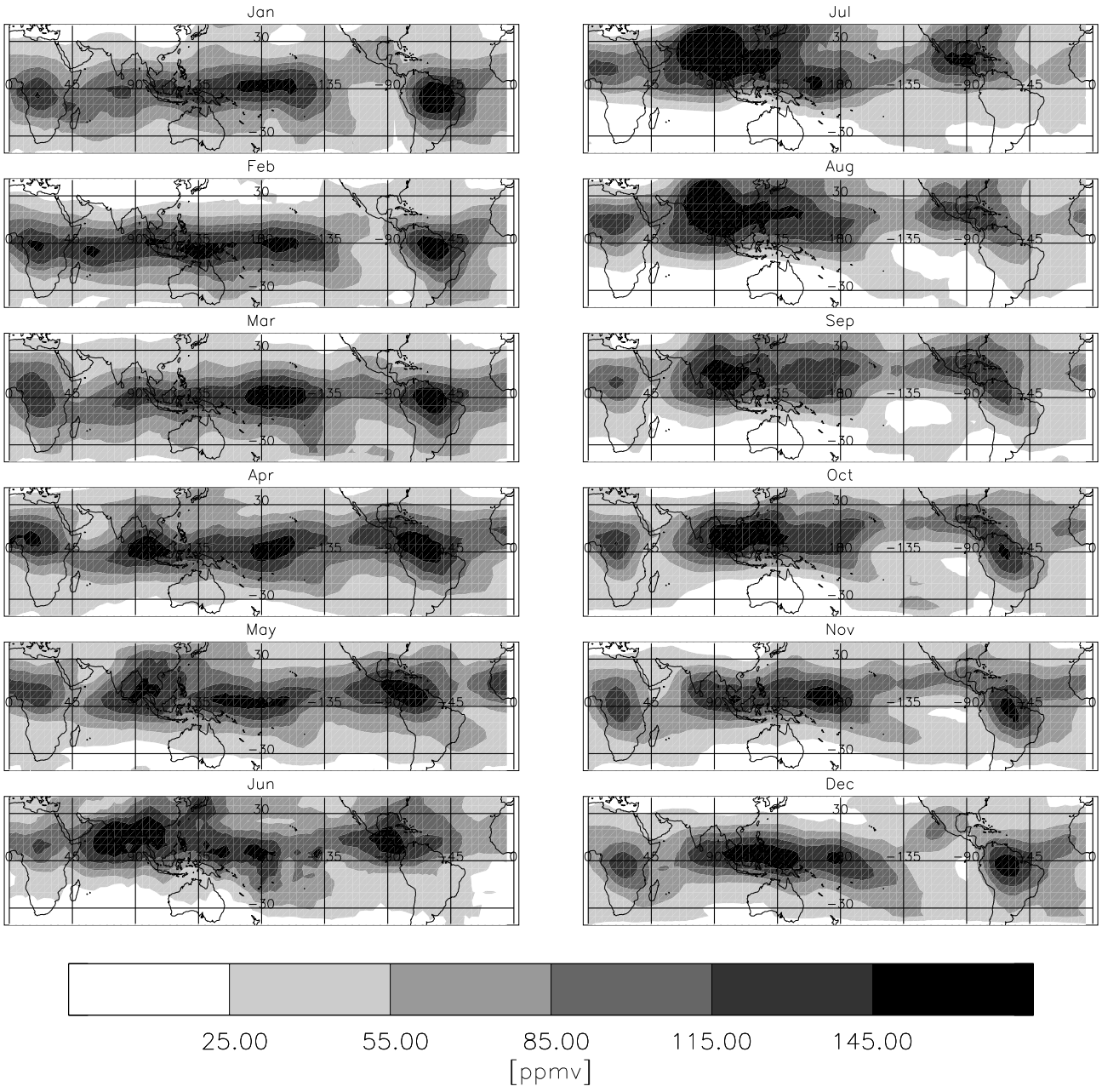
Jan
Feb
Mar
Apr
May
Jun
Jul
Aug
Sep
Oct
Nov
Dec
25.00
55.00
85.00
115.00
145.00
[ppmv]

Figure 6: Monthly averaged MLS mixing ratio (ppmv) at 215 hPa for January–December 1992. Mixing ratios have been produced from relative humidity using the ECMWF temperatures.

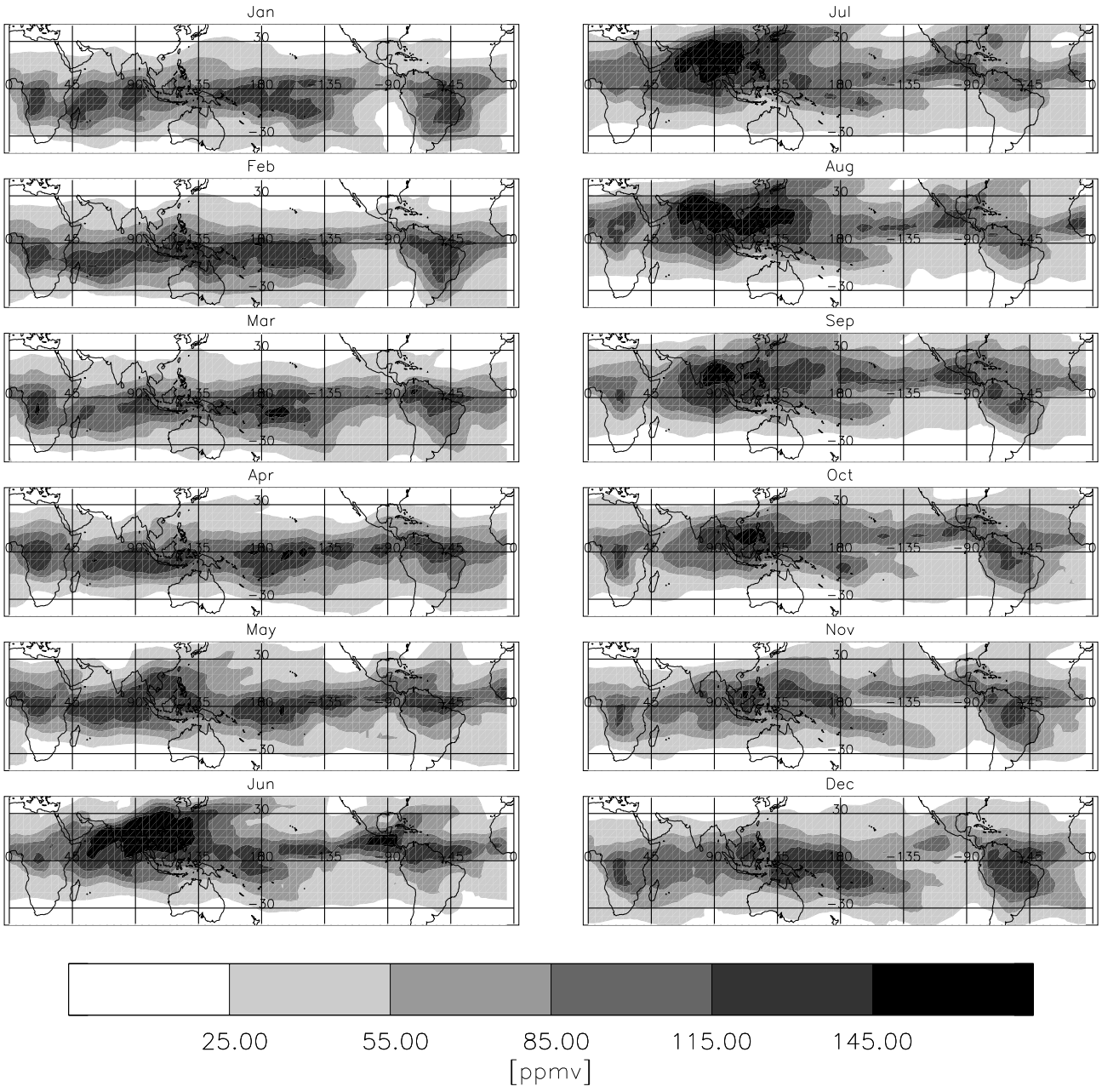
Jan
Feb
Mar
Apr
May
Jun
Jul
Aug
Sep
Oct
Nov
Dec
30
0
45
90
135
180
−135
−90
−45
−30
25.00
55.00
85.00
115.00
145.00
[ppmv]

Figure 7: Monthly averaged ECMWF mixing ratio (ppmv) at 215 hPa for January–December 1992. ECMWF relative humidities were multiplied by the MLS vertical averaging kernel and ECMWF temperatures were used in conversion to mixing ratio as in figure 6.

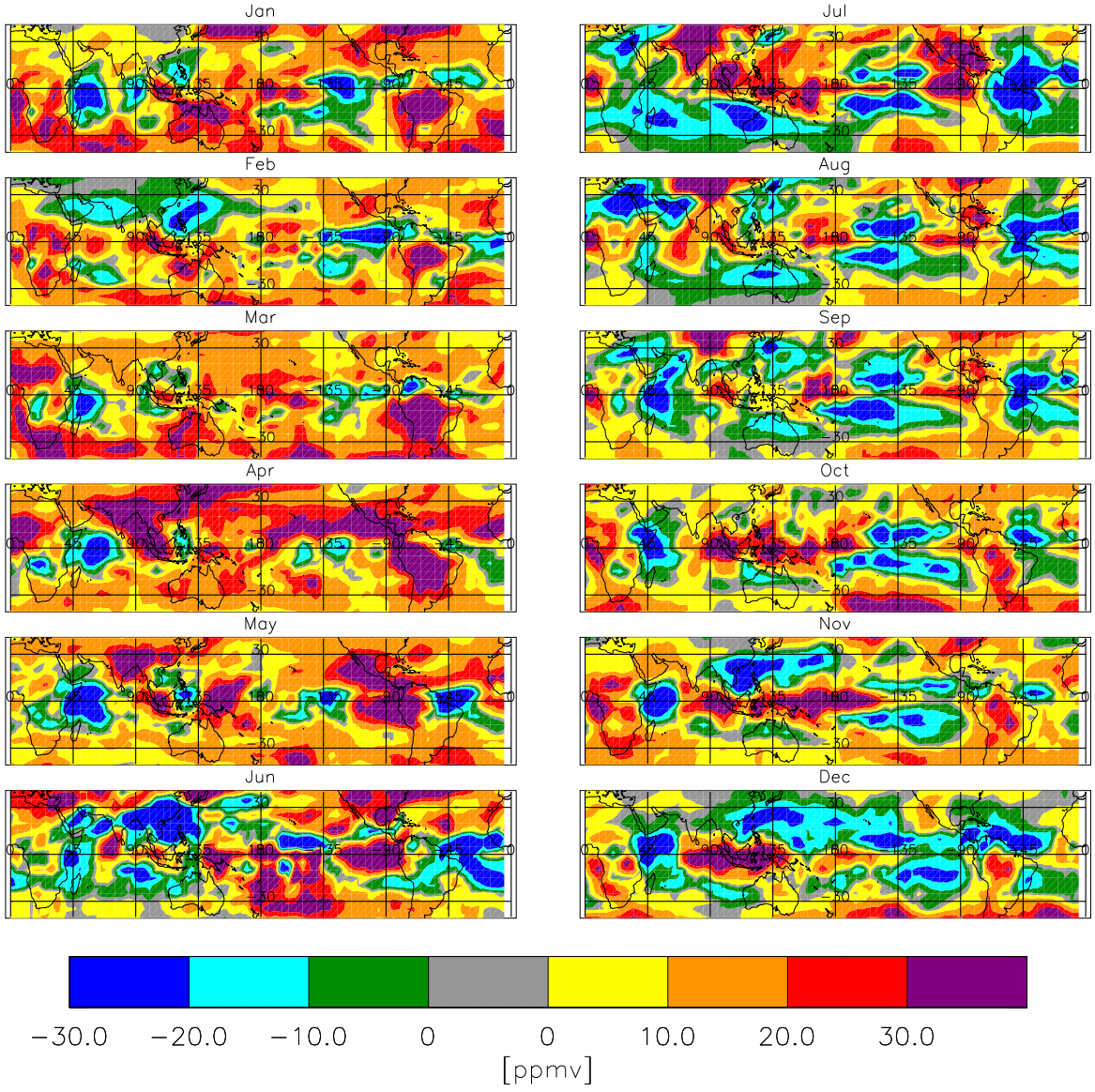
Jan
Feb
Mar
Apr
May
Jun
Jul
Aug
Sep
Oct
Nov
Dec
−30.0
−20.0
−10.0
0
0
10.0
20.0
30.0
[ppmv]

Figure 8: MLS minus ECMWF monthly averaged mixing ratio (ppmv) at 215 hPa for January–December 1992.

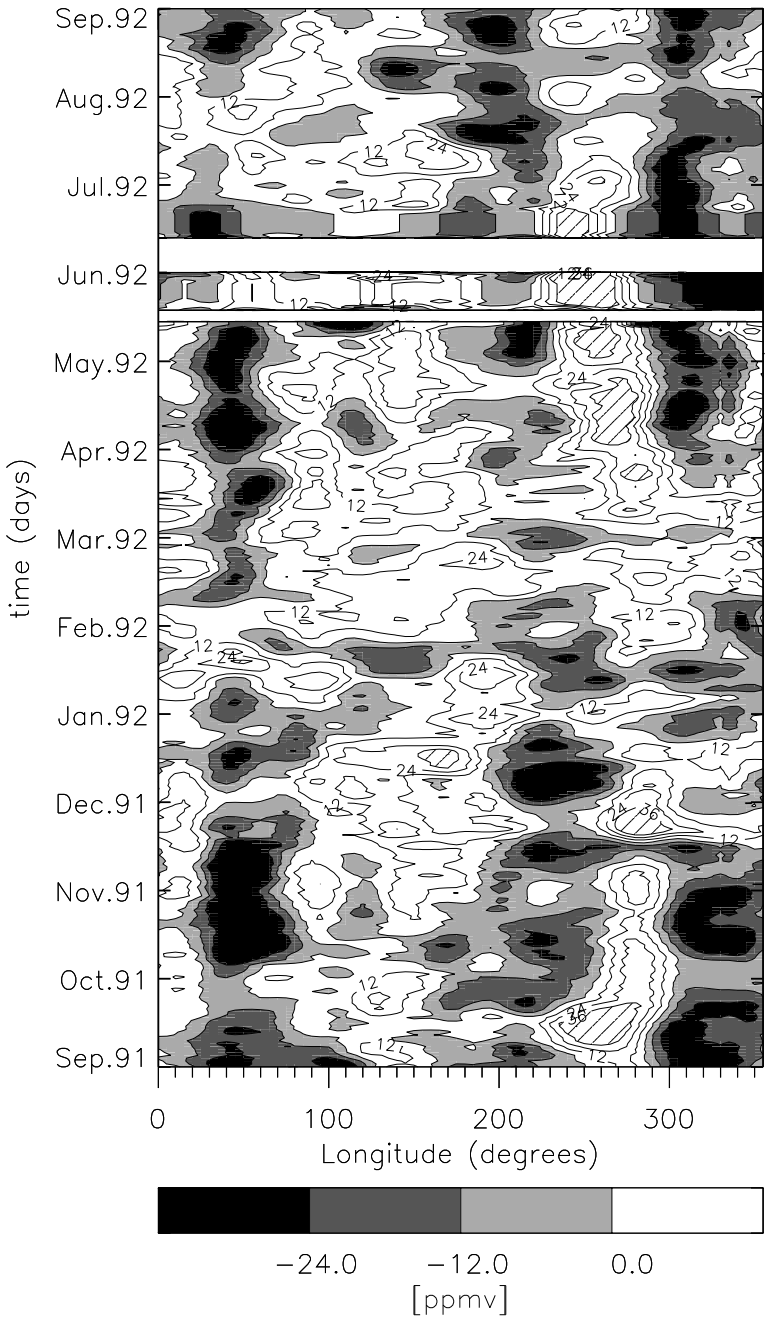
Sep.92
Aug.92
Jul.92
Jun.92
May.92
Apr.92
Mar.92
Feb.92
Jan.92
Dec.91
Nov.91
Oct.91
Sep.91
time (days)
0
100
200
300
Longitude (degrees)
−24.0
−12.0
0.0
[ppmv]

Figure 9: Longitude-time section showing the difference (MLS-ECMWF) in mixing ratio at the equator and 215 hPa. Contour interval is every 12 ppmv with values less than zero shaded, and values greater than 36 ppmv hatched.